Available online at www.sciencedirect.com
ScienceDirect
International Journal of Heat and Mass Transfer 50 (2007) 3072–3089
International Journal of HEAT and MASS TRANSFER
www.elsevier.com/locate/ijhmt

Role of metallic and composite (ceramic–metallic) supports on microwave heating of porous dielectrics

K. Aparna, Tanmay Basak, A.R. Balakrishnan *

Department of Chemical Engineering, Indian Institute of Technology Madras, Chennai 600 036, India

Received 19 August 2006; received in revised form 10 November 2006
Available online 1 February 2007

Abstract

The heating of porous dielectrics, beef–air (b/a) and beef–oil (b/o), attached with ceramic, metallic or ceramic–metallic composite supports, has been studied analytically using microwaves. Three test porosities were considered, 0.3, 0.45 and 0.6. A preliminary understanding of enhanced heating and power absorption within the material was obtained from the average power vs slab depth plots. The maxima in power, also termed as 'resonances', are observed for specific sample thicknesses and the two consecutive resonances are termed as R_1 and R_2 modes. It is observed that, for both b/a and b/o samples, higher intensity of resonances for power absorption occur in the presence of metallic and alumina–metallic composite supports. The detailed spatial distribution of power illustrates that the sample attached with the metallic support attains lower power distribution for both b/a and b/o samples. The low power absorption near the unexposed face has been enhanced by ceramic–metallic composite support. The overall heating efficiency is also enhanced with ceramic–metallic composite supports. The optimal heating strategy has been derived based on large heating rate with small thermal runaway. Metallic support may be recommended as optimal heating strategy for higher porosities ($\phi \geqslant 0.45$) whereas alumina–metallic composite support may be suitable for smaller porosities ($\phi \leqslant 0.45$) for b/a samples. Metallic or alumina–metallic composite supports give optimal heating effects for b/o samples. For both b/a and b/o samples, the thermal runaway is larger at higher porosities.

1. Introduction

Microwaves are electromagnetic waves in the frequency range 300 MHz to 300 GHz. Microwaves propagate through materials and the accompanying transport processes result in dissipation of electric energy into heat, which led to the term 'volumetric heat generation'. Due to volumetric effects microwaves are used extensively for thermal processing in various operations such as baking, concentrating, cooking, curing, thawing-tempering, and many more. Dielectric response of various materials play an important role in carrying out efficient material processing and a significant amount of earlier research was devoted to understand the physics of microwave assisted transport and heating characteristics. Microwaves are widely preferred over conventional heating due to shorter processing times. In conventional heating, heat is radiated from the burner to the surface of the material and the material is heated due to surface heat flux. In contrast, during microwave heating, the material dielectric loss which is a function of frequency of microwaves, is responsible for the conversion of electric energy to heat.

A significant amount of theoretical studies has been carried out by earlier researchers of microwaves [1–4] to understand spatial power and temperature distributions within samples. Ayappa et al. [1,2] carried out detailed theoretical analyses for microwave heating of 1D slabs and 2D cylinders. Transient temperature profiles were predicted within multilayered slabs and cylinders of dielectric materials by simultaneously solving Maxwell's equation and heat equation. Further studies have been carried out on resonances due to microwave propagation [3,4]. At a resonant condition the average power absorption within the sample is a local maximum and the effect of sample size on

* Corresponding author. Tel.: +91 44 2257 4154; fax: +91 44 2257 0509.
E-mail addresses: tanmay@iitm.ac.in (T. Basak), arbala@iitm.ac.in (A.R. Balakrishnan).

0017-9310/$ - see front matter © 2006 Elsevier Ltd. All rights reserved.
doi:10.1016/j.ijheatmasstransfer.2006.11.021

Nomenclature

$A_{x,l}$	amplitude of stationary wave for lth layer, V m^{-1}
A	Ampere
Bi	Biot number, –
c_p	specific heat capacity, J kg^{-1} K^{-1}
c	velocity of light, m s^{-1}
E_x	electric field intensity, V m^{-1}
f	frequency, Hz
H_y	magnetic field intensity, A m^{-1}
Im	imaginary part
k	thermal conductivity, W m^{-1} K^{-1}
k	propagation constant
L	half-slab thickness, m
L_s	sample thickness, m
q	microwave source term, W m^{-3}
Q	dimensionless microwave source term
Re	real part
t	time, s
T	temperature, K
u	dimensionless field component
v	dimensionless real field component
V	volt
w	dimensionless imaginary field component
z	distance, m
z'	dimensionless distance

Greek symbols

γ	dimensionless propagation constant
ϵ_0	free space permittivity, F m^{-1}
θ	dimensionless temperature
κ'	relative dielectric constant
κ''	relative dielectric loss
κ^*	relative complex dielectric properties
λ_m	wavelength in the medium, m
ρ	density, kg m^{-3}
ϕ	porosity, –
τ	dimensionless time
$\delta_{x,l}$	phase difference in stationary wave for lth layer
ω	angular frequency, rad s^{-1}

Subscripts

c	continuous phase
d	dispersed phase
eff	effective property
l	layer number

Superscripts

t	transmitted wave
r	reflected wave

enhanced microwave heating rate was analyzed in the presence of resonances by Barringer et al. [3] and Ayappa et al. [4]. Microwave heating and transport models were further applied for thawing and heating of multiphase systems in recent investigations [5–9] and greater rates in material processing were observed due to resonances. All these earlier works on heating and melting were carried out to investigate the heating effects solely due to the materials. Typically, materials are kept with a support in an oven or waveguide, and therefore, the foreign materials may interfere with the heating scenarios in the sample.

Basak and Priya [10] investigated the role of ceramic supports on microwave heating of materials with low and high dielectric loss (oil and water). A generalized heating strategy for materials due to uniform plane waves was derived. A theoretical analysis of microwave heating of food slabs supported by ceramic plates was also carried out by Basak and Meenakshi [11,12]. Their study involves processing of beef with oil layers with or without support for various cases. They also studied the effect of one side heating and distributed heating strategies for heating of low and high dielectric loss materials (beef and oil). Common to all these studies, is microwave heating of pure or non-porous substances.

Typical food systems may be realistically characterized as porous substances and the dielectric response of the porous substance would be non-trivial due to the effective dielectric properties of solid matrix and the fluid occupying the void space. Earlier studies on microwave heating of porous systems were carried out for several applications. Microwaves have been used for fabrication of ceramics [14,15]. Oh et al. [14] carried out fabrication of porous alumina in the presence of microwaves and Wang et al. [15] used microwave sintering for fabrication and characterization of porous ceramics. Microwaves have also been used for drying of materials [16–19]. Lyons et al. [16] carried out an experimental investigation of drying of a porous medium with internal heat generation. Drying of unsaturated porous materials was numerically and experimentally studied by Ratanadecho et al. [18]. Use of combined heating for drying of porous materials was studied by experimental investigation by Glouannec et al. [17]. This work was extended by Salagnac et al. [19] when they developed a numerical model for combined hot air, infrared and microwave drying of a porous material and experimental and simulated values were compared. Various models have been developed to describe heat transfer processes in porous systems. Ni et al. [20] developed a multiphase porous media model to predict moisture transport during intensive microwave heating of porous biomaterials. The effects of microwave heating of a batch fluidized bed was investigated by solving a coupled heat and mass transfer model by Chen et al. [21]. Wang and Sun [22] have reviewed the recent developments in numerical modeling of heating

and cooling processes in the food industry. A multiphase porous media model has also been developed by Dincov [23] to predict the heating mechanism for intensive microwave heating of porous materials. Datta [24] developed a general multiphase model which described a number of heat and mass transfer processes in foods, particularly those involving internal evaporation. However, the distribution of microwave power absorption within the porous bed due to effective dielectric response was absent in these analyses. Recently, the effect of ceramic supports on microwave heating of porous dielectrics was investigated by Basak et al. [13]. They studied heating of porous samples in presence of various distributions of microwaves and an efficient heating strategy was developed. However, this work was limited to studies involving microwave heating of samples supported on ceramic plates alone. Realistically, food substances can be supported on various ceramic/metallic substances when they are heated using microwaves. In the current work an analysis has been presented for microwave heating of porous samples supported on metallic and composite metallic–ceramic plates.

The present work attempts to study the heating effects of typical food substances (porous beef) with metallic, ceramic and composite supports in the presence of microwaves. The analysis has been carried out in the presence of resonances or maxima in power within the sample for various porosity regimes. During resonances, material absorbs greater power and the presence of a support may alter the power absorption within the material. The analysis involves two typical porous materials such as beef–air (b/a) and beef–oil (b/o) where air or oil is assumed to be the fluid medium of the porous body. The dielectric response is modeled using effective dielectric properties for various porosity values. The resonating phenomena is quite complicated for material-support complex and a detailed investigation on resonances for such material-support (metallic or ceramic–metallic composite) has been carried out to achieve efficient heating strategies for material processing. The role of traveling waves within the porous body and various supports on the heating rates are analyzed. The efficient heating mechanism characterized by 'maxima in temperature rise with minimal thermal

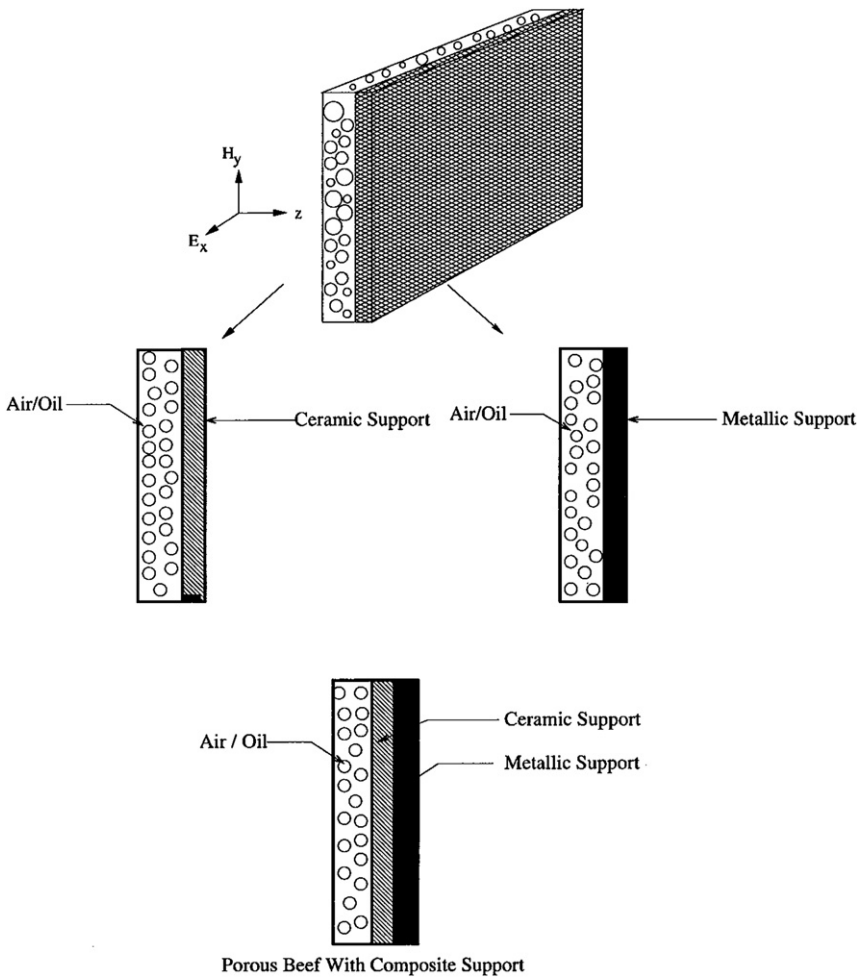

Fig. 1. Schematic illustration of a porous dielectric beef sample exposed to a plane electromagnetic wave. Two cases of porous dielectrics are considered: beef–air (b/a) and beef–oil (b/o).

runaway effects' has been illustrated for both beef–air (b/a) and beef–oil (b/o) samples with various porosity regimes.

2. Theory

2.1. Microwave propagation in porous multilayered dielectric with metallic and ceramic supports

The porous dielectric with ceramic/metallic support may be represented as a one dimensional slab. Similar assumptions are also found in earlier literature [5–11]. The wave propagation due to uniform electric field, E_x, obtained from Maxwell's equation is

$$\frac{d^2E_x}{dz^2} + k^2E_x = 0, \tag{1}$$

where E_x lies in x–y plane and varies only in the direction of propagation, z-axis (Fig. 1). It may be noted that, $k = \frac{\omega}{c}\sqrt{\kappa' + i\kappa''}$ is the propagation constant which depends on the dielectric constant, κ' and the dielectric loss, κ''. Note that $\omega = 2\pi f$, where f is the frequency of the electromagnetic wave and c is the velocity of light. In a n multilayered sample the equation for wave propagation due to electric field for the lth layer obtained from Eq. (1) is

$$\frac{d^2E_{x,l}}{dz^2} + k_l^2E_{x,l} = 0, \tag{2}$$

where $z_{l-1} \leqslant z \leqslant z_l$ and $l = 1, \ldots, n$. Assuming that each layer has constant dielectric properties, the general solution to Eq. (2) represented as a linear combination of transmitted and reflected waves propagating in opposite directions is

Table 1
Thermal and dielectric properties for air, oil, raw beef, Al_2O_3 and SiC [10,11,18]

Material property	Air	Oil	Raw beef	Al_2O_3	SiC
Heat capacity, c_p ($J\,kg^{-1}\,K^{-1}$)	1158.93	2000	2510	1046	3300
Thermal conductivity, k ($Wm^{-1}\,K^{-1}$)	0.0706	0.168	0.491	26	40
Density, ρ ($kg\,m^{-3}$)	0.325	900	1070	3750	3100
Dielectric constant, κ' (2450 MHz)	1.0	2.8	43	10.8	26.66
Dielectric loss, κ'' (2450 MHz)	0.0	0.15	15	0.1566	27.99

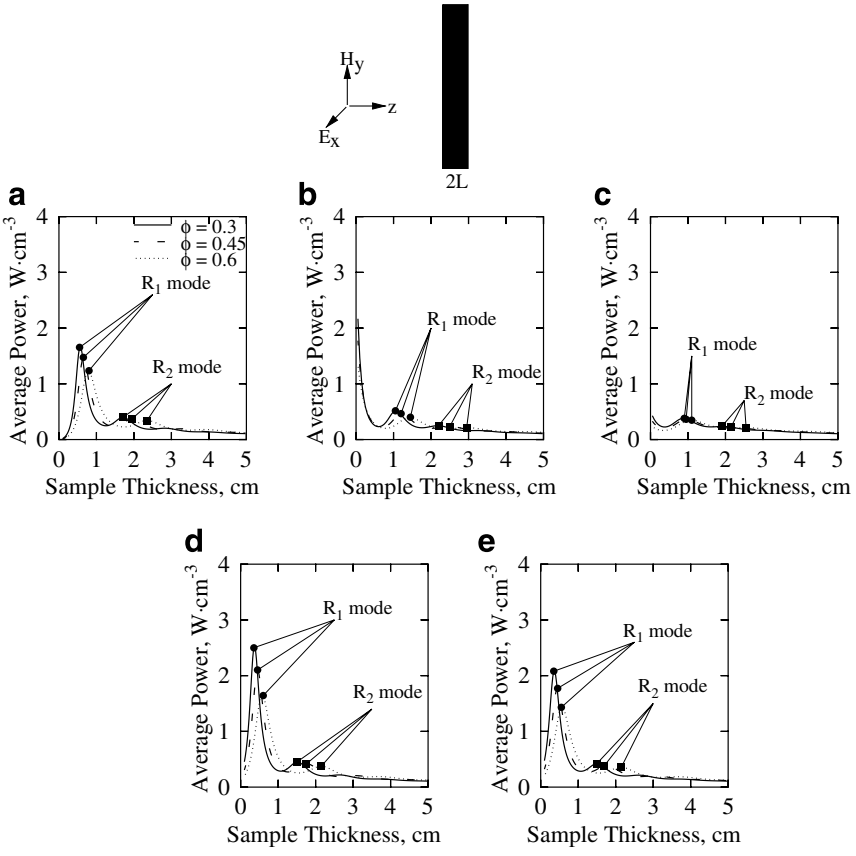

Fig. 2. Average power ($W\,cm^{-3}$) vs sample thickness (cm) for beef–air (b/a) samples with (a) metallic support, (b) alumina support, (c) SiC support, (d) alumina–metallic support and (e) SiC–metallic support with porosities $\phi = 0.3$, 0.45 and 0.6 exposed to microwaves at the left face. The symbol, ●, denotes R_1 mode and the symbol, ■, denotes R_2 mode of resonances.

$$E_{x,1} = E_{\mathrm{t},1}e^{ik_1 z} + E_{\mathrm{r},1}e^{-ik_1 z}$$

First or air layer,

$$E_{x,l} = E_{\mathrm{t},l}e^{ik_l z} + E_{\mathrm{r},l}e^{-ik_l z} \tag{3}$$

Porous media and support $l = 2, \ldots, n-1$,

where $E_{\mathrm{t},l}$ and $E_{\mathrm{r},l}$ are the coefficients due to transmission and reflection respectively.

$$E_{x,n} = \begin{cases} E_{\mathrm{t},n}e^{ik_n z} + E_{\mathrm{r},n}e^{-ik_n z} & \text{(air)}, \\ 0 & \text{(metallic support)}, \end{cases} \tag{4}$$

The boundary conditions at the interface are

$$\left.\begin{aligned} E_{x,l-1} &= E_{x,l} \\ \frac{\mathrm{d}E_{x,l-1}}{\mathrm{d}z} &= \frac{\mathrm{d}E_{x,l}}{\mathrm{d}z} \end{aligned}\right\} \begin{aligned} &l = 2, \ldots, n, \\ &z = z_1, \ldots, z_{n-1}, \end{aligned} \tag{5}$$

Here $z_1, z_2, \ldots, z_{n-1}$ denote the boundaries between interfaces.

The interface conditions (Eq. (5)) and the general solutions (Eqs. (3) and (4)) are used to obtain the coefficients, $E_{\mathrm{t},l}$ and $E_{\mathrm{r},l}$ by solving the set of algebraic equations.

$$\left.\begin{aligned} &E_{\mathrm{t},l}e^{ik_l z_l} + E_{\mathrm{r},l}e^{-ik_l z_l} - E_{\mathrm{t},l+1}e^{ik_{l+1} z_l} \\ &\quad - E_{\mathrm{r},l+1}e^{-ik_{l+1} z_l} = 0 \\ &k_l E_{\mathrm{t},l}e^{ik_l z_l} - k_l E_{\mathrm{r},l}e^{-ik_l z_l} - k_{l+1}E_{\mathrm{t},l+1}e^{ik_{l+1} z_l} \\ &\quad + k_{l+1}E_{\mathrm{r},l+1}e^{-ik_{l+1} z_l} = 0 \end{aligned}\right\} l = 1, \ldots, n-1. \tag{6}$$

As the incident field intensities from the left and right are known, i.e. $E_{\mathrm{t},1} = E_0$ and $E_{\mathrm{r},n} = 0$, Eq. (6) are solved for the remaining $2n-2$ coefficients using MATLAB [7,8,10]. For the lth layer, the transmitted and reflected waves are

$$\begin{aligned} E^{\mathrm{t}}_{x,l} &= E_{\mathrm{t},l}e^{ik_l z} = A^{\mathrm{t}}_{x,l}e^{i\delta^{\mathrm{t}}_{x,l}}, \\ E^{\mathrm{r}}_{x,l} &= E_{\mathrm{r},l}e^{-ik_l z} = A^{\mathrm{r}}_{x,l}e^{i\delta^{\mathrm{r}}_{x,l}}, \end{aligned} \tag{7}$$

where corresponding amplitudes are given by

$$\begin{aligned} A^{\mathrm{t}}_{x,l} &= \sqrt{E^{\mathrm{t}}_{x,l}E^{\mathrm{t}\,*}_{x,l}}, \\ A^{\mathrm{r}}_{x,l} &= \sqrt{E^{\mathrm{r}}_{x,l}E^{\mathrm{r}\,*}_{x,l}} \end{aligned} \tag{8}$$

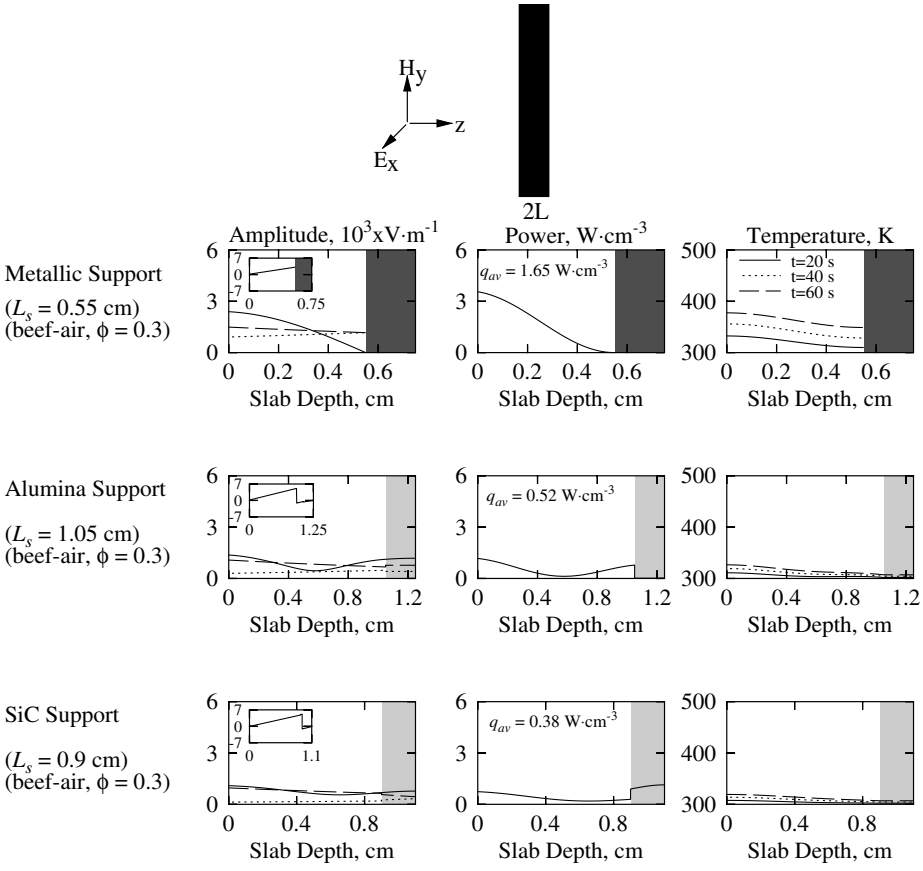

Fig. 3. Amplitudes of electric field $(A_{x,l}, A^{\mathrm{t}}_{x,l}, A^{\mathrm{r}}_{x,l})$, power distributions and temperature profiles for beef–air (b/a) samples with metallic, alumina and SiC supports for porosity $\phi = 0.3$ exposed to microwaves from the left face during R_1 mode. — —, transmitted wave; · · ·, reflected wave; —, stationary wave. The inset shows phase difference $(\delta_{x,l})$ vs z.

and the phase states are given by

$$\delta^{t}_{x,l} = \tan^{-1}\left[\frac{\mathrm{Im}(E^{t}_{x,l})}{\mathrm{Re}(E^{t}_{x,l})}\right],$$
$$\delta^{r}_{x,l} = \tan^{-1}\left[\frac{\mathrm{Im}(E^{r}_{x,l})}{\mathrm{Re}(E^{r}_{x,l})}\right], \quad (9)$$

where the superscript, '*' in Eq. (8) denotes the complex conjugate. For a stationary wave in the lth layer, the amplitude is given by

$$A_{x,l} = \sqrt{E_{x,l}E^{*}_{x,l}} \quad (10)$$

and the difference in phase angle is given by

$$\delta_{x,l} = \delta^{t}_{x,l} - \delta^{r}_{x,l}, \quad (11)$$

where the quantities $E_{x,l}$ and $E^{*}_{x,l}$ in Eq. (10) are evaluated using Eqs. (3), (4) and (7). At the resonance, the difference in phase angle is zero, i.e., $\delta_{x,l} = 0$. The absorbed power in lth layer, obtained from Poynting vector theorem is

$$q_l(z) = \frac{1}{2}\omega\epsilon_0\kappa''_{\mathrm{eff}}(\phi)E_{x,l}(z)E^{*}_{x,l}(z). \quad (12)$$

Here ϵ_0 is the free space permittivity, ϕ is the porosity and κ''_{eff} is the effective dielectric loss where,

$$\kappa_{\mathrm{eff}}(\phi) = \kappa'_{\mathrm{eff}}(\phi) + \mathrm{i}\kappa''_{\mathrm{eff}}(\phi) \quad (13)$$

and for a porous medium, the effective dielectric properties κ_{eff} can be obtained from Fricke's complex conductivity model [25]:

$$\kappa_{\mathrm{eff}} = \frac{\kappa^{*}_{c}[\kappa^{*}_{d}(1+a\phi) + a\kappa^{*}_{c}(1-\phi)]}{\kappa^{*}_{d}(1-\phi) + \kappa^{*}_{c}(a+\phi)} \quad (14)$$

Here κ^{*}_{c} and κ^{*}_{d} are the relative complex dielectric properties of the continuous (beef) and dispersed (air/oil) phases respectively. It may be noted that $a = 2$ for spherical dispersions and $a = 1$ for cylindrical dispersions. Based on experimental observations, $a = 2$ is chosen for this study.

The average power obtained by integrating the power across the slab is

$$\bar{q} = \frac{1}{2L}\int_{-L}^{+L} q_l(z)\,\mathrm{d}z \approx \frac{1}{2L}\sum_{z=0}^{2L} q_l(z). \quad (15)$$

Here $-L$ and L denote the left and right faces of the slab respectively and $q_l(z)$ denotes the power as a function of z where z may be measured from the left edge of the slab or sample. It may be noted that, $2L$ is the thickness of the entire slab consisting of sample and supports. L_s is the thickness of the sample and L' is the total thickness of the support such that $2L = L_s + L'$. The average power for a sample of thickness L_s is

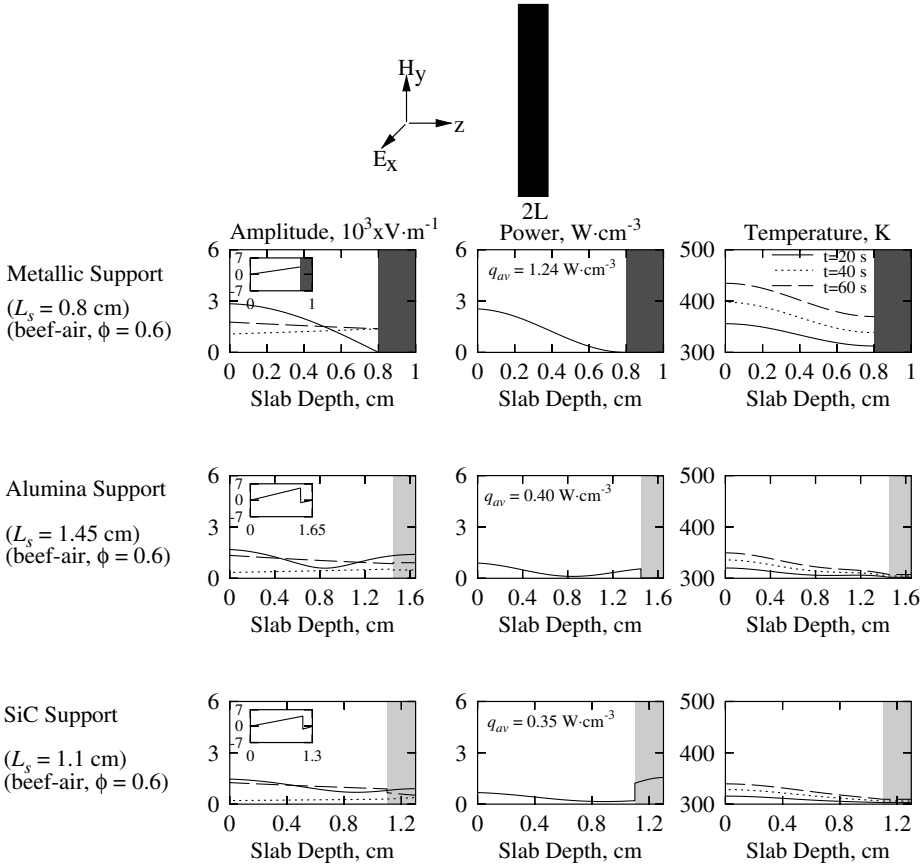

Fig. 4. Amplitudes of electric field $(A_{x,l}, A^{t}_{x,l}, A^{r}_{x,l})$, power distributions and temperature profiles for beef–air (b/a) samples with metallic, alumina and SiC supports for porosity $\phi = 0.6$ exposed to microwaves from the left face during R_1 mode. — —, transmitted wave; ···, reflected wave; —, stationary wave. The inset shows phase difference $(\delta_{x,l})$ vs z.

$$q_{\mathrm{av}} = \frac{1}{n}\sum_{i=1}^{n} q_l(z_i) \quad \text{for } 0 \leqslant z_i \leqslant L_{\mathrm{s}}. \tag{16}$$

2.2. Modeling of microwave heating and solution strategy

The energy balance equation for heating of a porous dielectric by microwave radiation is

$$\rho c_p \frac{\partial T}{\partial t} = k\frac{\partial^2 T}{\partial z^2} + q(z), \tag{17}$$

where ρ, the effective density, c_p, the effective specific heat capacity and k, the effective thermal conductivity and are given by

$$\rho = (1-\phi)\rho_{\mathrm{c}} + \phi\rho_{\mathrm{d}}, \tag{18}$$

$$c_p = (1-\phi)c_{p_{\mathrm{c}}} + \phi c_{p_{\mathrm{d}}} \tag{19}$$

and

$$k = (1-\phi)k_{\mathrm{c}} + \phi k_{\mathrm{d}}. \tag{20}$$

It may be noted that the subscripts 'c' and 'd' represent the continuous and dispersed phases, respectively. The density ρ in Eq. (18) describes the effective density and it is assumed to be uniform bulk density throughout the sample. The volumetric heat source, in Eq. (17), $q(z)$ is defined as in Eq. (12). In a n multilayered sample, the energy balance equation for the lth layer obtained from Eq. (17) is

$$(\rho c_p)_l \frac{\partial T_l}{\partial t} = k_l \frac{\partial^2 T_l}{\partial z^2} + q_l(z) \quad l = 1, \ldots, n \tag{21}$$

The boundary conditions are

$$k_1 \frac{\partial T_1}{\partial z} = 0 \quad z = z_1 \tag{22}$$

and

$$-k_{n-1}\frac{\partial T_{n-1}}{\partial z} = 0 \quad z = z_{n-1}, \tag{23}$$

The interface conditions between phase interfaces are

$$\left.\begin{aligned} T_l &= T_{l+1} \\ k_l \tfrac{\partial T_l}{\partial z} &= k_{l+1}\tfrac{\partial T_{l+1}}{\partial z} \end{aligned}\right\} \begin{aligned} &l = 2, \ldots, n-2 \\ &z = z_2, \ldots, z_{n-2} \end{aligned} \tag{24}$$

The wave propagation equation for a particular medium is given in Eq. (2). As microwave power, $q_l(z)$ is a function of electric field as seen in Eq. (12), a functional representation of electric field is necessary to solve the energy balance equation (Eq. (21)). The evaluation of functional form of electric field is difficult for a multilayered sample.

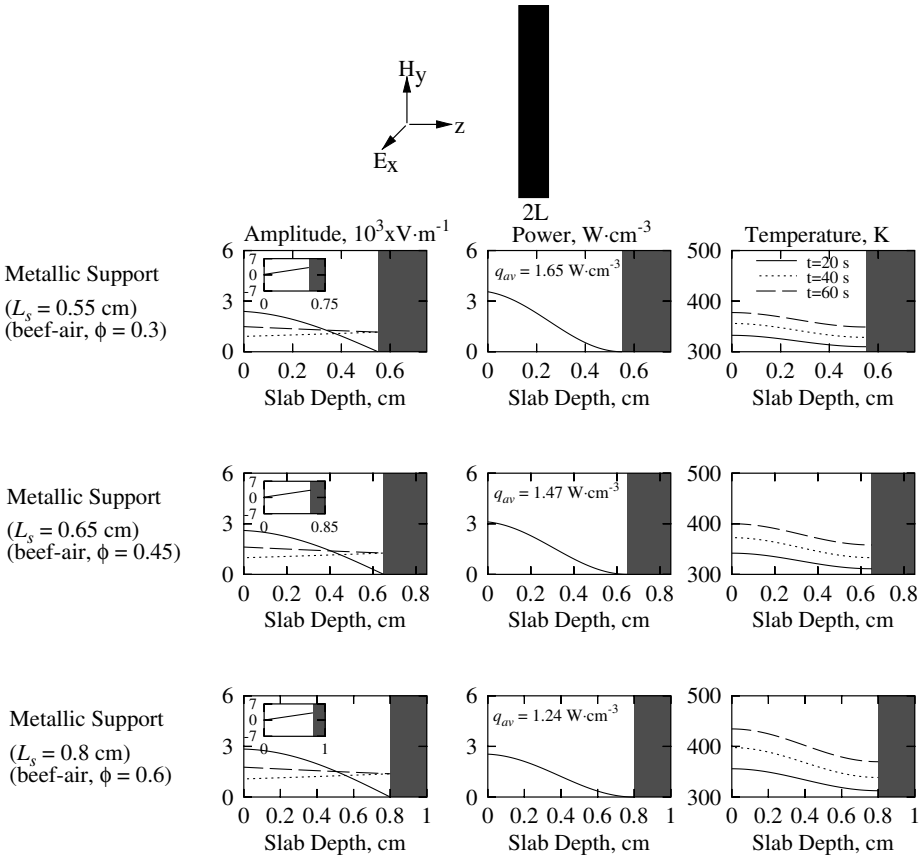

Fig. 5. Amplitudes of electric field $(A_{x,l}, A^{\mathrm{t}}_{x,l}, A^{\mathrm{r}}_{x,l})$, power distributions and temperature profiles for beef–air (b/a) samples with metallic support for porosities, $\phi = 0.3$, 0.45 and 0.6 exposed to microwaves from the left face during R_1 mode. — —, transmitted wave; ···, reflected wave; —, stationary wave. The inset shows phase difference $(\delta_{x,l})$ vs z.

Alternatively, the energy balance and wave equations (Eqs. (21) and (2)) are solved numerically.

The dielectric properties are obtained from Table 1. It may be noted that dielectric properties correspond to microwave frequency 2450 MHz. The porous dielectric substance may be represented by either beef–air or beef–oil (see Fig. 1). The typical values of porosities 0.3, 0.45 and 0.6 are considered for the computation. The microwave incidence is assumed to be from left side of the sample as seen in Fig. 1. The temperature of the sample and support is 300 K at $t = 0$ s. The thickness of the sample varies between 0.1 and 5 cm and a thickness of support of 0.2 cm for all test cases has been assumed. Al_2O_3 is a transparent medium and SiC absorbs microwave significantly [26]. It is assumed smaller thickness of support and influence of various thicknesses of support on microwave heating of materials may not be important.

The energy balance equation and the electric field equations with the appropriate boundary conditions are solved using Galerkin finite element method. The interface conditions for energy balance and electric field equations due to multiple phases are automatically satisfied via an interface element common to two phases. At the interface node, the field variable and fluxes are continuous as discussed by Reddy [27] and Ayappa et al. [1]. To discretize the time domain, Crank–Nicholson method is used, and the nonlinear residual equations are solved using Newton Raphson Method [7,8]. Due to the lack of a good initial guess to begin the Newton scheme, a small time step $\Delta t = 1 \times 10^{-4}$ s was used in the first step. Unless specified otherwise $\Delta t = 0.1$ s was used for subsequent steps and typically 25–50 quadratic elements were used. It was found that the maximum difference for the values of the unknowns at the nodes was less than 1% when the values were compared for 25 and 50 elements. Similarly the maximum difference was less than 1% when the results were compared for $\Delta t = 0.05$ s and 0.1 s.

3. Results and discussion

3.1. Microwave power and temperature distributions for beef–air samples

A preliminary study has been carried out to analyze the role of metallic and ceramic supports on microwave heating of porous dielectrics via the average power vs sample thickness diagram. Note that in all cases, the sample is exposed to a microwave radiation of intensity 1 W cm^{-2}. The maxima in average power is often termed as resonances and the two consecutive resonances may be referred

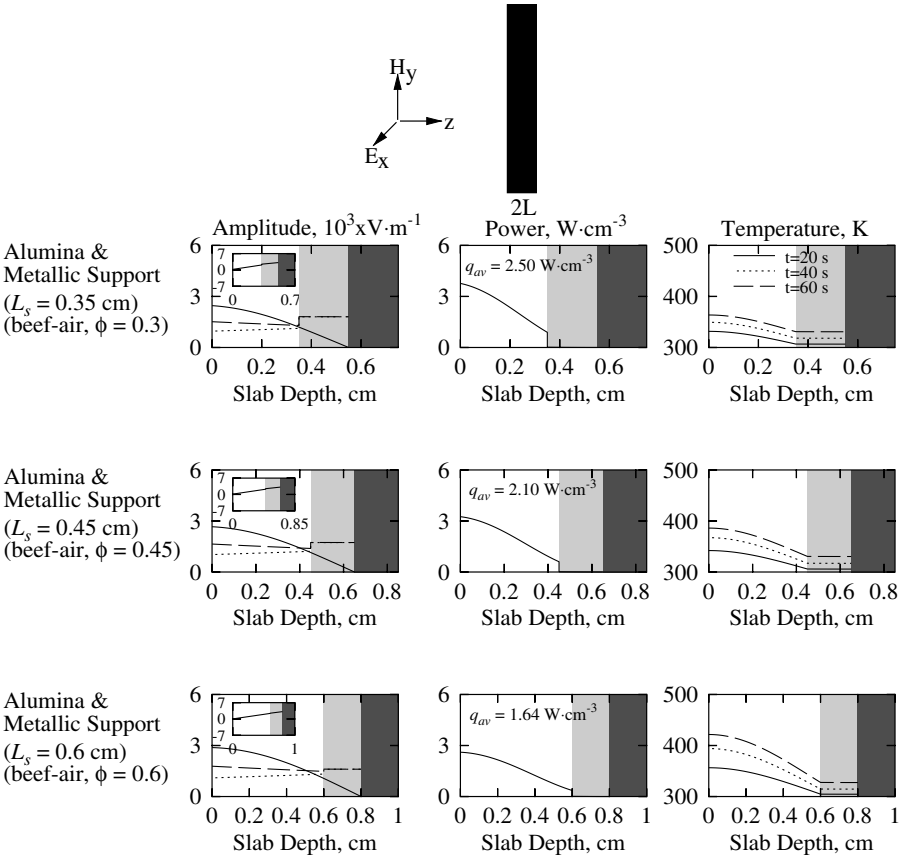

Fig. 6. Amplitudes of electric field ($A_{x,l}, A^{t}_{x,l}, A^{r}_{x,l}$), power distributions and temperature profiles for beef–air (b/a) samples with alumina–metallic composite support for porosities, $\phi = 0.3$, 0.45 and 0.6 exposed to microwaves from the left face during R_1 mode. — —, transmitted wave; ⋯, reflected wave; —, stationary wave. The inset shows phase difference ($\delta_{x,l}$) vs z.

to as R_1 and R_2 modes. The significant resonances occur at two consecutive R_1 and R_2 modes. The resonances R_1 and R_2 are due to constructive interferences between transmitted and reflected waves and the amplitudes of the transmitted and reflected waves are generally larger for smaller sample dimensions corresponding to the R_1 mode. Hence, the average power at R_1 mode is generally greater than that at R_2 mode irrespective of the materials. Fig. 2a–e illustrates the average power vs sample thickness diagram for samples with metallic, ceramic (alumina and SiC) and composite (alumina–metallic and SiC–metallic) supports. Note that, the wavelength of microwaves for beef–air for the three porosities are 2.33, 2.70 and 3.22 cm, respectively.

It is observed from Fig. 2a that largest average power corresponds to beef–air with porosity $\phi = 0.3$ and average power decreases as porosity increases during both R_1 and R_2 modes for samples with metallic support. It is also observed that the average power is greater during R_1 mode for all the three porosity cases. In addition, the sample thickness corresponding to R_1 and R_2 modes is found to increase as porosity increases. A similar pattern of average power with porosities is observed for microwave heating of samples with ceramic and composite supports and the support may play a significant role on microwave heating as seen in Fig. 2a–e. Fig. 2b shows that average power during R_1 mode is much smaller than that for metallic support as seen in Fig. 2a for all porosities. It may be noted that the average power of beef sample with metallic support for porosity $\phi = 0.3$ during R_1 mode is 1.65 W cm^{-3} whereas it is 0.52 W cm^{-3} for samples with alumina support, 0.38 W cm^{-3} with SiC support, 2.5 W cm^{-3} with alumina–metallic support and 2.08 W cm^{-3} with SiC–metallic support. It is interesting to note that for all three porosities, beef sample with alumina–metallic composite support corresponds to the largest average power and the sample with SiC support corresponds to the smallest average power for R_1 mode.

An efficient use of supports depends on factors such as faster thermal processing, porosity of the beef sample and controlled or uniform thermal processing. The interesting features as seen in Fig. 2a–e thus provide the stimulus for determining the role of supports on efficient heating of beef samples using microwaves. A detailed analysis of microwave power characteristics and electric field distributions at various resonance modes would be useful to understand the interference of waves and the critical role of the specific support on food/material processing.

Fig. 3 illustrates the spatial distribution of amplitude, power and temperature for beef–air samples with metallic and ceramic supports with porosity $\phi = 0.3$ during R_1

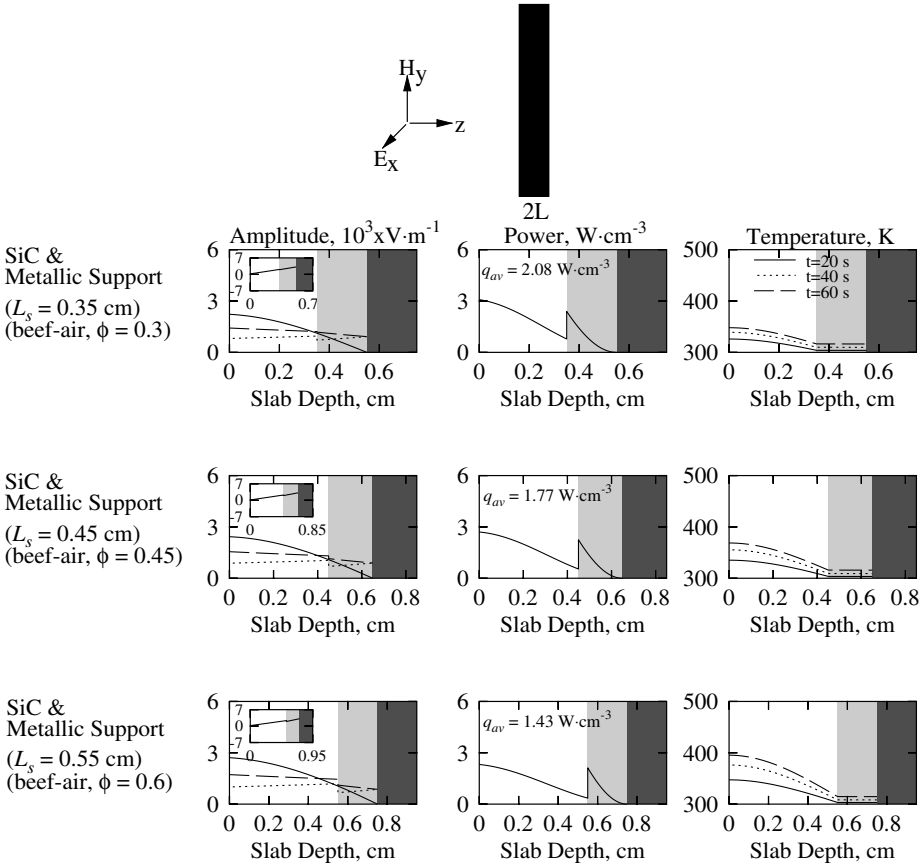

Fig. 7. Amplitudes of electric field $(A_{x,l}, A^{t}_{x,l}, A^{r}_{x,l})$, power distributions and temperature profiles for beef–air (b/a) samples with SiC–metallic composite support for porosities, $\phi = 0.3$, 0.45 and 0.6 exposed to microwaves from the left face during R_1 mode. — —, transmitted wave; ···, reflected wave; —, stationary wave. The inset shows phase difference $(\delta_{x,l})$ vs z.

mode. For all these cases, the slab depth (L_s) corresponding to R_1 mode are 0.55, 1.05 and 0.9 cm for sample with metallic support, alumina support and SiC support, respectively. It is observed that amplitude of the transmitted wave is a decreasing function of distance whereas the amplitude of the reflected wave is an increasing function within the sample for all the cases. The difference in phase angle vs distance within the slabs illustrates the strength of the stationary wave and zero phase difference signifies constructive interference, which is also termed as resonance (see inset). It is also observed that the amplitude of the transmitted and reflected waves are identical near the metallic support. Although the amplitudes are equal in the sample near the metallic support, the destructive interference as illustrated by the phase shift between $-\pi$ and π (see inset) occurs at the unexposed face resulting in zero electric field. The stationary electric field forms a maxima at the exposed face for the sample with metallic support. The metallic support does not allow the waves to penetrate through and significant amount of reflection would cause stronger stationary waves within the sample. The interference of waves within the sample is also quite strong resulting in greater power absorption throughout the sample except at the unexposed face. The power profile follows the same trend as the stationary electric field and the average power for metallic support is 1.65 W cm^{-3}.

The amplitude of the stationary electric field has two maxima occurring at the surfaces when the sample is attached to alumina support unlike the one spatial resonance that occurs with metallic support. The waves do penetrate through and reflect out of the ceramic supports and thus the interference of waves within the sample are coupled with propagation of waves in ceramic supports. Therefore, the stationary waves within the sample are weaker than those within the sample with metallic support. It is also observed that, due to smaller dielectric loss of alumina support ($\kappa'' = 0.1566$), the microwave power absorption is quite small within the support. In contrast, due to greater dielectric loss of SiC ($\kappa'' = 27.99$), significant power absorption occurs within SiC support. The role of SiC support may be illustrated by the fact that more transmission and reflection within the support may decrease the amplitudes of traveling waves within the sample. The power profile follows the same trend as the stationary electric field for ceramic supports. Due to significant reflection within the metallic support, power absorbed within the sample is larger than that with ceramic supports.

The spatial distributions of temperature within the sample during 20, 40 and 60 s have also been illustrated in Fig. 3. The temperature varies within 316–348 K for the sample with metallic support during 60 s whereas it varies within 307–326 K for alumina support and within 307–

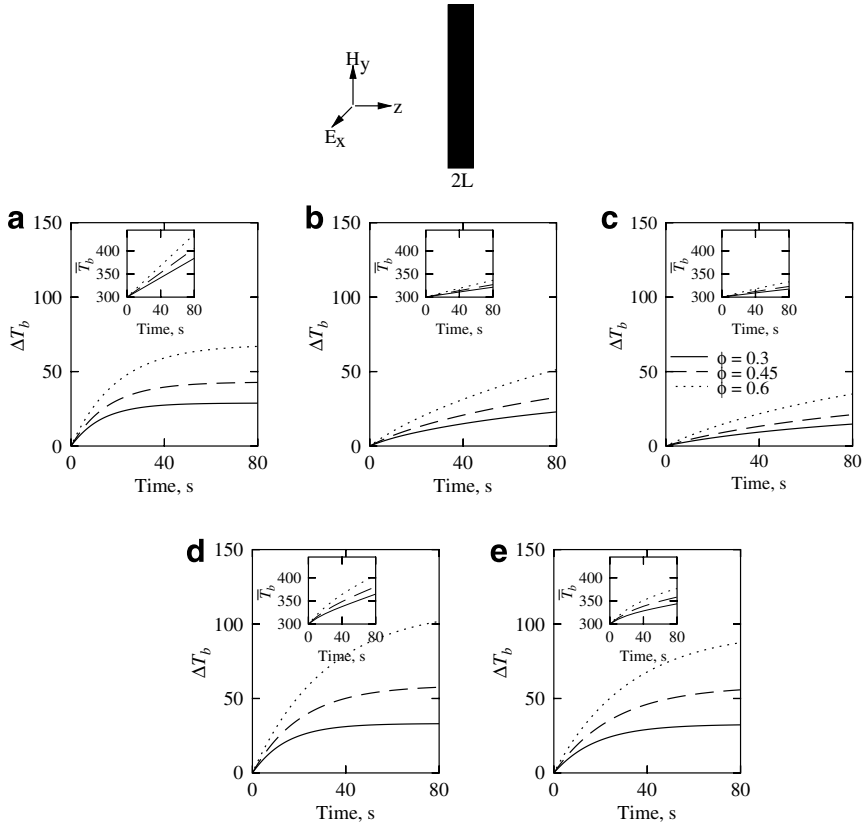

Fig. 8. The temperature difference, ΔT_b (K) vs time (s) for porous beef–air samples ($\phi = 0.3$, 0.45 and 0.6) exposed to microwaves at one face during R_1 mode for (a) metallic support, (b) alumina support, (c) SiC support, (d) alumina–metallic support, (e) SiC–metallic support. The inset shows average temperature, $\overline{T}_b$ (K) vs time (s).

319 K for SiC support. The greater temperature distributions with the metallic support are due to greater power distributions which is in contrast with ceramic supports. It is interesting to note that, although the power at the regime near the metallic support is almost zero, the temperature profile is significantly high, due to the larger thermal conductivity of the beef sample. Similar to metallic support, the temperature at the exposed face is larger than that at the unexposed face for ceramic supports.

Fig. 4 shows the amplitude, power and temperature distributions for beef–air samples with metallic and ceramic supports for porosity $\phi = 0.6$ during R_1 mode. The amplitudes of traveling waves within the sample and supports are qualitatively similar to sample with porosity 0.3. As in Fig. 3, the electric field is zero near the metallic support. It is noted that, the stationary electric field forms a maxima at the exposed face for metallic support, whereas for alumina and SiC supports, two maxima are formed at the exposed and unexposed faces. It may be noted that, the slab depths are 0.8, 1.45 and 1.1 cm for metallic, alumina and SiC support cases, respectively. It is interesting to note that the samples with porosity $\phi = 0.6$ correspond to greater sample thickness than that with porosity $\phi = 0.3$. The power absorption for the three support cases are 1.24, 0.40 and 0.35 W cm^{-3} respectively, whereas the absorbed power for beef with porosity $\phi = 0.3$ are 1.65, 0.52 and 0.38 W cm^{-3} respectively. It may be noted that the absorbed power for porosity $\phi = 0.6$ is less than that for $\phi = 0.3$ for metallic and ceramic supports. Similar to beef with porosity 0.3, the average power within the beef sample is higher for metallic support than that with ceramic supports. Fig. 4 also illustrates the spatial distribution of temperature within the sample during 20, 40 and 60 s. It is seen that, the temperatures for metallic and ceramic supports are higher than that for samples with porosity $\phi = 0.3$ (Fig. 3). The temperatures during 60 s varies within 370–434 K, 307–349 K and 309–339 K respectively for metallic, alumina and SiC supports, whereas the temperatures are 316–348 K for metallic support, 307–326 K for alumina support and 307–319 K for SiC support for $\phi = 0.3$. It may be observed that the temperature distribution increases as porosity increases and larger porosity corresponds to smaller average power.

A comparison of power and temperature distributions for various porosities with metallic support is shown in Fig. 5 with the spatial distribution of amplitude, power and temperature for samples with metallic support during R_1 mode for the three porosities, 0.3, 0.45 and 0.6, respectively. The sample thicknesses are 0.55, 0.65 and 0.8 cm for $\phi = 0.3$, 0.45 and 0.6, respectively. It is observed that the

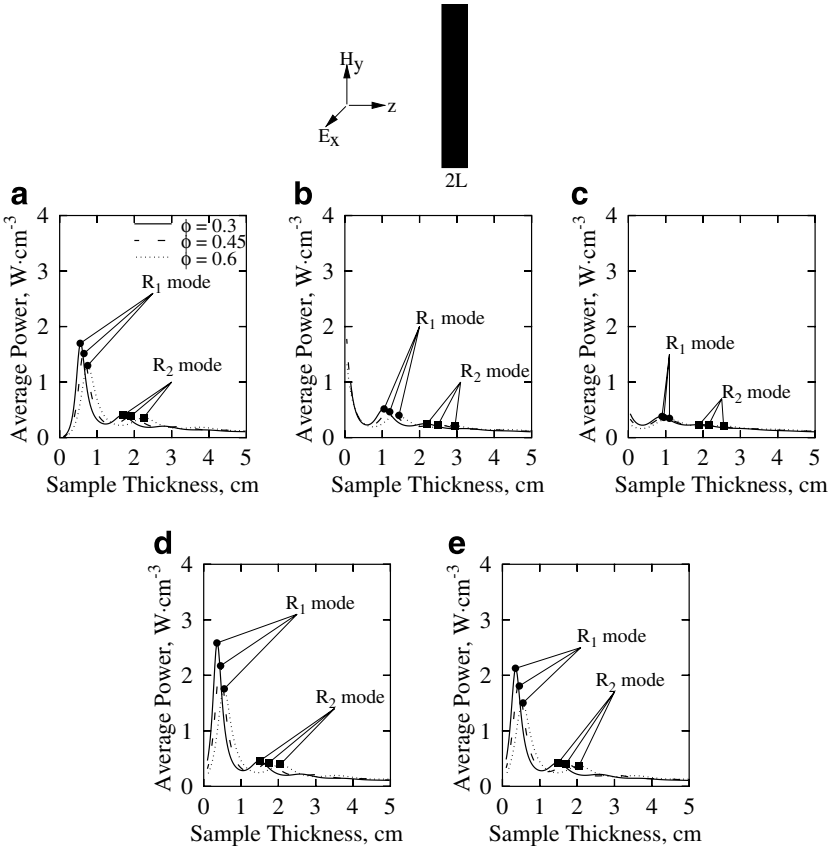

Fig. 9. Average power (W cm^{-3}) vs sample thickness (cm) for beef–oil (b/o) samples with (a) metallic support, (b) alumina support, (c) SiC support, (d) alumina–metallic support, (e) SiC–metallic support for porous beef with porosities $\phi = 0.3$, 0.45 and 0.6 exposed to microwaves at one face. The symbol, ●, denotes R_1 mode and the symbol, ■, denotes R_2 mode of resonances.

amplitude of the transmitted wave is a decreasing function of distance within the sample while amplitude of the reflected wave is an increasing function of distance within the sample, for all porosity ranges. It is seen that the amplitude of the transmitted and reflected waves are identical near the metallic support. Although the amplitudes are equal at the sample face attached to the metallic support, the destructive interference illustrated by the phase shift as seen in the inset, occurs at the unexposed face resulting in zero electric field. The distribution of amplitudes of both the transmitted and reflected waves are greater for beef sample with $\phi = 0.6$ whereas the sample with $\phi = 0.3$ exhibits the larger spatial distribution of power due to greater dielectric loss (κ''). The average powers (q_{av}) are 1.65, 1.47 and 1.24 W cm^{-3} for the three porosities, respectively. Values of $\kappa'' = 9.13$, 6.73 and 4.61 for $\phi = 0.3$, 0.45 and 0.6, respectively.

The spatial temperature distributions are illustrated for $t = 20$, 40 and 60 s. The temperature distributions qualitatively follow the power distributions. At $\phi = 0.6$, which corresponds to the smallest average power, the highest temperature distribution due to smaller effective heat capacity is noticed. The specific heat capacities are 2104.67, 1902 and 1699 J kg^{-1} K^{-1} respectively for the three porosities $\phi = 0.3$, 0.45 and 0.6, respectively.

Effect of ceramic–metallic composite supports on enhancement of power absorption has been analyzed in detail for various porosities in Figs. 6 and 7. In addition, situation of zero power absorption due to metallic support can be improved by using the ceramic–metallic composite support. Fig. 6 illustrates the spatial distribution of amplitude, power and temperature for sample with alumina–metallic composite support during R_1 mode. It is observed that a maxima in stationary field and power occurs at the exposed face of the sample, as in the case of metallic support (Fig. 5). There is a significant jump in amplitude of the transmitted and reflected wave within the alumina support, especially for $\phi = 0.3$ and 0.45. As in the case of metallic support, the amplitude of the traveling and stationary waves are slightly larger for $\phi = 0.6$. In addition, the presence of alumina–metallic composite support seems to enhance the amplitudes of the waves within the sample and therefore the larger spatial power distributions are observed for sample with specific porosities. It may be noted that the average power absorption (q_{av}) within the beef sample are 2.5, 2.1 and 1.64 W cm^{-3} for $\phi = 0.3$, 0.45 and 0.6, respectively with alumina–metallic support whereas $q_{av} = 1.65$, 1.47 and 1.24 W cm^{-3} respectively for metallic support with similar porosities. Although the composite support gives larger average power, the total power

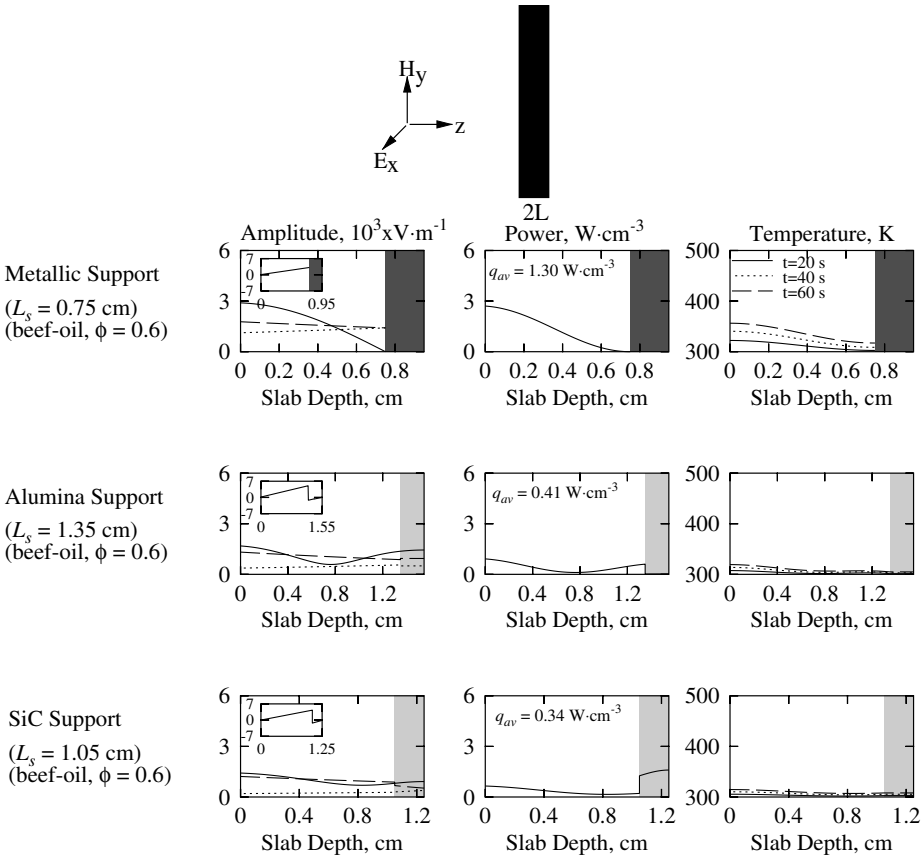

Fig. 10. Amplitudes of electric field ($A_{x,l}, A^{t}_{x,l}, A^{r}_{x,l}$), power distributions and temperature profiles for beef–oil (b/o) samples with metallic, alumina and SiC supports for porosity $\phi = 0.6$ exposed to microwaves from the left face during R_1 mode. — —, transmitted wave; ···, reflected wave; —, stationary wave. The inset shows phase difference ($\delta_{x,l}$) vs z.

absorption is larger with metallic support. The slab depth (L_s) with composite support corresponding to R_1 mode is smaller than that with metallic support. The value of $L_s = 0.35$, 0.45 and 0.6 cm for $\phi = 0.3$, 0.45 and 0.6, respectively for the composite support.

The temperature distributions are illustrated for $t = 20$, 40 and 60 s in Fig. 6. The temperature at the exposed face is higher than that at the unexposed face. The temperatures are within 331–363 K, 330–386 K and 327–421 K, respectively for $\phi = 0.3$, 0.45 and 0.6 for composite support whereas the temperatures are within 349–377, 358–400 and 370–435 K for metallic support. As with the metallic support, the temperature at the exposed face increases with increase in porosity.

Fig. 7 shows the spatial distribution of amplitude, power and temperature for beef with SiC–metallic composite support during R_1 mode. As in Fig. 6, the sample thicknesses in this case are $L_s = 0.35$, 0.45 and 0.55 cm for $\phi = 0.3$, 0.45 and 0.6, respectively during R_1 mode. As in earlier cases, the amplitudes of the transmitted and reflected waves increase with increase in porosity. The amplitude of the reflected wave within the sample is smaller due to the presence of SiC support and therefore, the strength of the stationary wave within the sample is reduced. In addition, the smaller power within the sample may be due to greater power absorption within the SiC support due to the fact that SiC support has a greater dielectric loss. As a result, power absorption within the sample is smaller than that with alumina–metallic support. It is interesting to note that even though the average power absorption within the sample with SiC–metallic support is smaller than that with alumina–metallic support, the average power is higher than that with metallic support. However, the total power absorption with SiC–metallic support is smaller than that with metallic support. The average power absorption with SiC–metallic support are 2.08, 1.77 and 1.43 W cm^{-3} for $\phi = 0.3$, 0.45 and 0.6, respectively. As in the earlier cases, the maxima in temperature is found to occur at the exposed face. The temperature within the sample varies within 316–348 K for $\phi = 0.3$, 316–368 K for $\phi = 0.45$ and 315–395 K for $\phi = 0.6$, at 60 s.

An efficient microwave heating policy is accompanied by maxima in heating rates with minimal thermal runaway. Fig. 8a–e shows temperature difference (ΔT_b) vs time distribution for beef with metallic, ceramic, and composite supports for the porosities 0.3, 0.45 and 0.6. ΔT_b is defined as the difference between the maximum and minimum temperatures within the sample. It can be seen that temperature difference increases with increase in porosity for all cases (Fig. 8). It is also observed that, the largest temperature

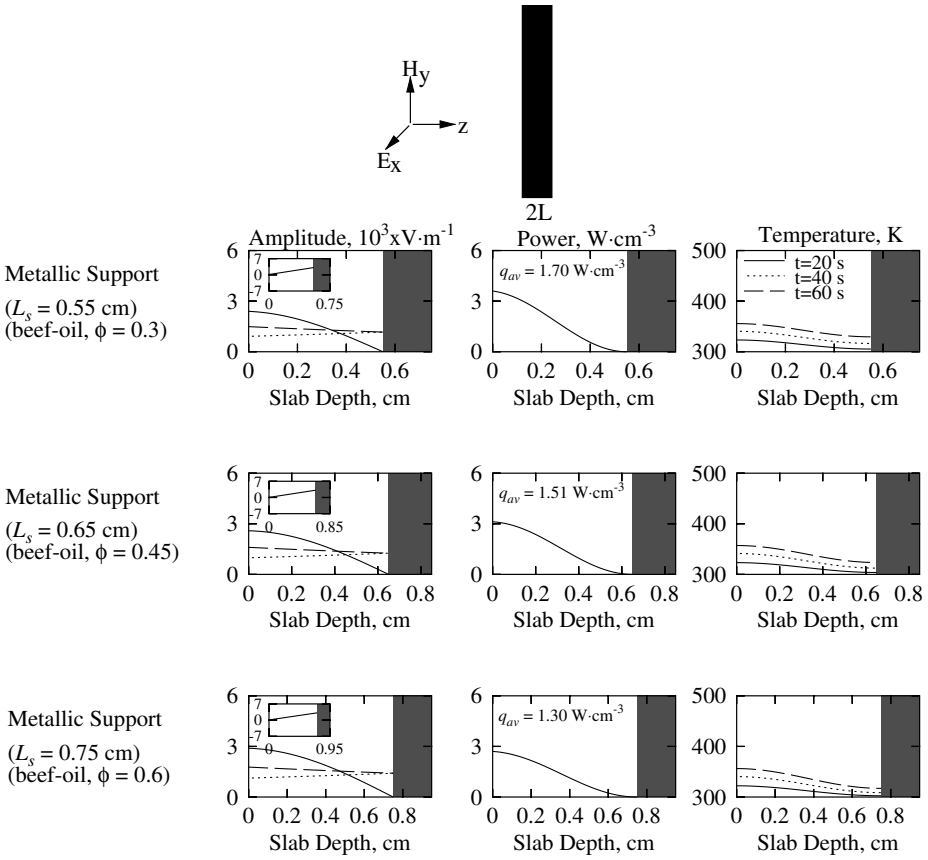

Fig. 11. Amplitudes of electric field ($A_{x,l}, A^t_{x,l}, A^r_{x,l}$), power distributions and temperature profiles for beef–oil (b/o) samples with metallic support for porosities, $\phi = 0.3$, 0.45 and 0.6 exposed to microwaves from the left face during R_1 mode. — —, transmitted wave; ···, reflected wave; —, stationary wave. The inset shows phase difference ($\delta_{x,l}$) vs z.

difference is found in the case of beef with alumina–metallic composite support, especially for higher porosities. For alumina–metallic support, the temperature difference (ΔT_b) is around 33 K for $\phi = 0.3$, 57 K for $\phi = 0.45$ and 101.7 K for $\phi = 0.6$ at 80 s, whereas ΔT_b is 28.7 K for $\phi = 0.3$, 42.7 K for $\phi = 0.45$ and 66.9 K for $\phi = 0.6$ for metallic support.

The inset shows the average temperature ($\overline{T}_b$) vs time plot where the slope of the plot represents the heating rate which is directly proportional to the microwave power absorption. It is observed that the average temperature distribution has larger slopes for higher porosities. The average temperature vs time curve is very steep for $\phi = 0.6$ for metallic support and alumina–metallic support (Fig. 8a and d). The average temperatures for $\phi = 0.6$ at 80 s are 436 K for metallic support, 405 K for alumina–metallic support, 377 K for SiC–metallic support, 336 K for alumina support and 333 K for SiC support. For lower porosity $\phi = 0.3$, the average temperatures are 384 K for metallic support, 365 K for alumina–metallic support, 344 K for SiC–metallic support, 321 K for alumina support and 317 K for SiC support. Therefore, an optimal heating strategy may be suggested as the metallic support for greater porosities ($\phi \geqslant 0.45$) and alumina–metallic support for smaller porosities ($\phi \leqslant 0.45$).

3.2. Microwave power and temperature distributions for beef–oil samples

Fig. 9a–e illustrates the average power vs sample thickness diagram for beef–oil sample with metallic, ceramic and composite supports, for three porosities, 0.3, 0.45 and 0.6. The distributions are qualitatively similar to beef–air case. As in Fig. 2, the highest average power corresponds to sample with composite supports, and average power is found to decrease with increase in porosity for all cases. As porosity increases, the sample thickness corresponding to R_1 and R_2 modes increases for all supports. As in beef–air sample, the highest average power corresponds to alumina–metallic support. The average power absorption with alumina–metallic support is 2.58 W cm^{-3}, whereas it is 2.12 W cm^{-3} with SiC–metallic support and 1.70 W cm^{-3} for metallic support corresponding to $\phi = 0.3$. The minimum average power corresponds to ceramic supports. The average power for the sample with SiC support corresponding to $\phi = 0.3$ is 0.38 W cm^{-3} and average power corresponding to $\phi = 0.6$ is 0.34 W cm^{-3}.

Fig. 10 shows the spatial distribution of amplitude, power and temperature for beef–oil samples with metallic and ceramic supports for the porosity, $\phi = 0.6$ during R_1 mode. It may be noted that, the sample with metallic

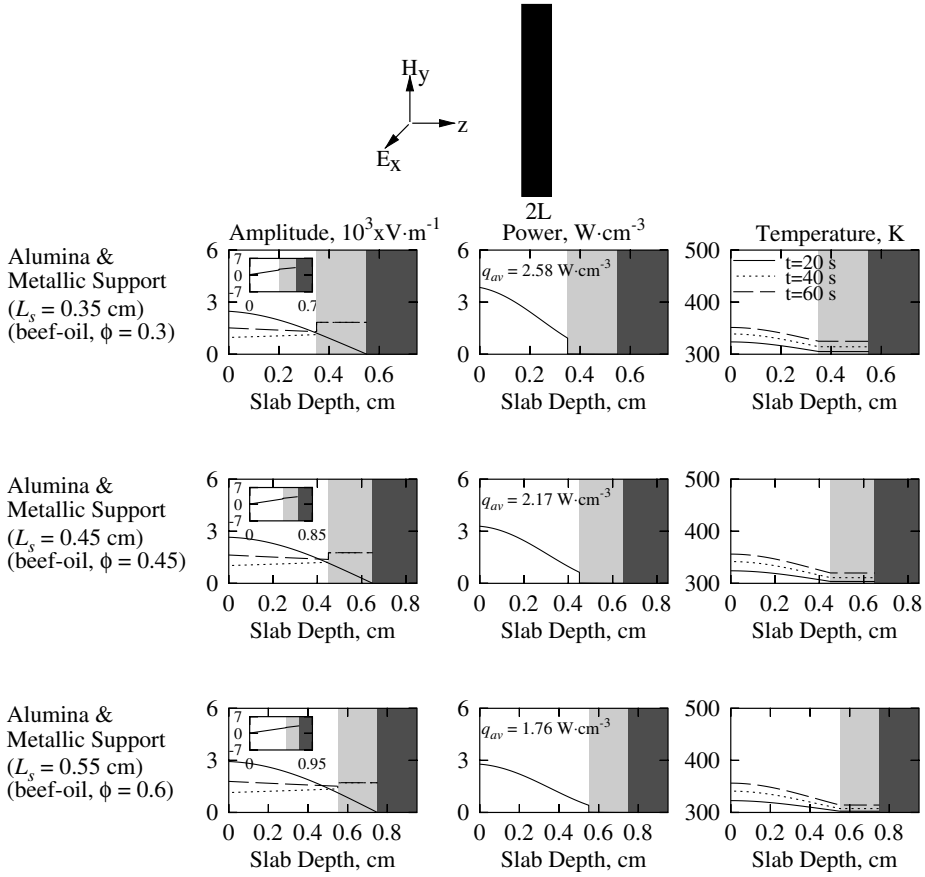

Fig. 12. Amplitudes of electric field ($A_{x,l}, A^t_{x,l}, A^r_{x,l}$), power distributions and temperature profiles for beef–oil (b/o) samples with alumina–metallic composite support for porosities, $\phi = 0.3$, 0.45 and 0.6 exposed to microwaves from the left face during R_1 mode. — —, transmitted wave; ···, reflected wave; —, stationary wave. The inset shows phase difference ($\delta_{x,l}$) vs z.

support shows a maxima in stationary electric field on the exposed face of the beef sample while alumina support shows two maxima in electric field on both faces. The power profile follows qualitatively the stationary electric field distribution. The sample with metallic support corresponds to the smallest sample thickness at R_1 mode. The sample thicknesses are 0.75 cm, 1.35 cm and 1.05 cm within the beef sample for metallic, alumina and SiC supports, respectively. As in the beef–air case, the amplitudes of the transmitted and reflected waves are equal in the sample regime near the metallic support. Further, as in the beef–air case with metallic support, destructive interference results in zero electric field at the unexposed end attached to the metallic support. The average power absorption within the sample with metallic support is 1.30 W cm^{-3}. The average power absorption is larger than that with ceramic supports. The average power absorption for alumina support is 0.41 W cm^{-3} and for SiC support it is 0.34 W cm^{-3}. As in the beef–air case (Fig. 4) the highest average power corresponds to metallic support whereas the lowest corresponds to SiC support. The temperature profile at 20, 40 and 60 s with metallic and ceramic supports are also shown. The temperature within the sample at 60 s varies from 317 to 356 K for metallic support case, 305 to 319 K for alumina support case and 308 to 315 K for SiC support case.

Fig. 11 shows the spatial distribution for beef–oil sample with metallic support for the three porosities 0.3, 0.45 and 0.6. The spatial distributions are qualitatively similar to Fig. 5 for all porosities. The slab depth for the three porosities are 0.55, 0.65 and 0.75 cm respectively. The power profile qualitatively follows the stationary electric field distributions. The average power absorptions for the three porosities are 1.70, 1.51 and 1.30 W cm^{-3}, respectively. As in Fig. 5, the power absorption in the sample layer very close to the metallic support is nearly zero. Similar to power profile, temperature profiles show a maxima at the exposed face. Although the power absorption in the regime near the metallic support is almost zero, the temperature profile shows a high value because of the higher thermal conductivity of beef–oil sample. The temperatures are 329–355 K for $\phi = 0.3$, 323–357 K for $\phi = 0.45$ and 317–356 K for $\phi = 0.6$ at $t = 60$ s. It may be interesting to note that, while power profile decreases with increase in porosity, the temperature variation remains almost the same for the three porosities.

Fig. 12 shows the spatial distribution of amplitude, power and temperature for beef–oil with alumina–metallic

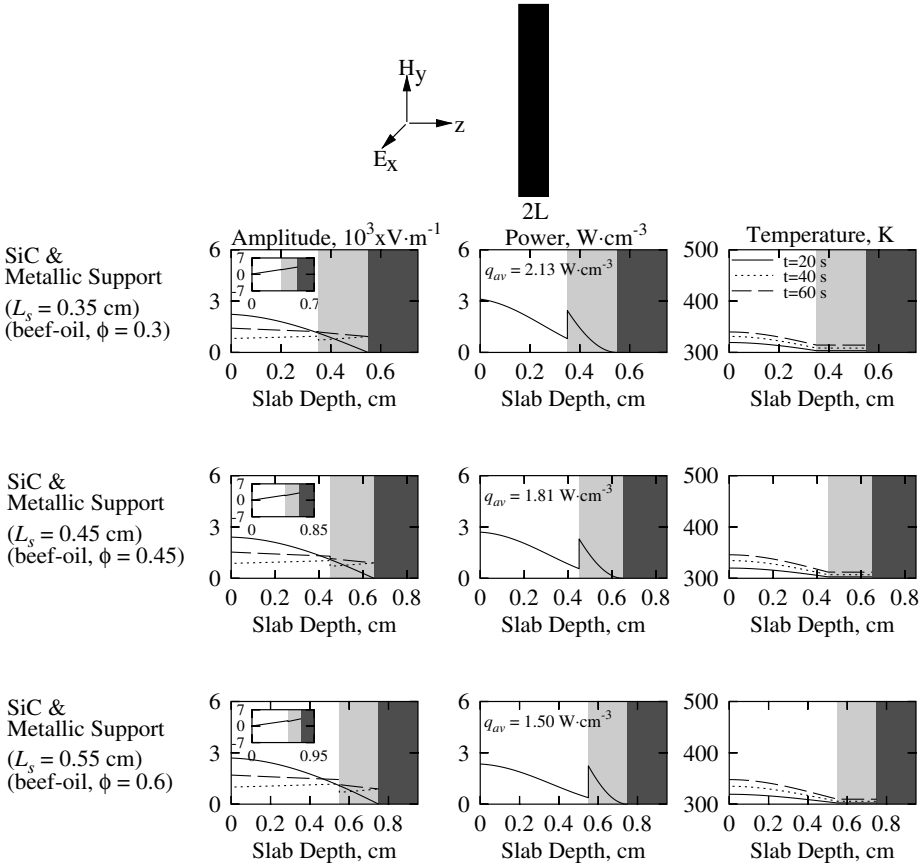

Fig. 13. Amplitudes of electric field ($A_{x,l}, A^{t}_{x,l}, A^{r}_{x,l}$), power distributions and temperature profiles for beef–oil (b/o) samples with SiC–metallic composite support for porosities, $\phi = 0.3$, 0.45 and 0.6 exposed to microwaves from the left face during R_1 mode. — —, transmitted wave; ···, reflected wave; —, stationary wave. The inset shows phase difference ($\delta_{x,l}$) vs z.

composite support. The sample thicknesses in this case are 0.35, 0.45 and 0.55 cm, respectively. There is a jump in amplitude of the transmitted and reflected waves at the sample–support interface due to the presence of ceramic support. A maxima in the amplitude of the stationary electric field is seen on the exposed face of the sample. Similarly, the power profile also shows a maxima on the exposed face. The average power absorption for sample with alumina–metallic support is significantly larger than that with metallic support. The average power absorption with the metallic support case are 1.70, 1.51, 1.30 W cm^{-3} whereas with alumina–metallic support, the average powers are 2.58, 2.17 and 1.76 W cm^{-3} for the three porosities. It may be noted that, similar to metallic support case, there is also a small variation in the temperature profile as porosity increases. The temperature varies within 325–351 K for $\phi = 0.3$, 320–356 K for $\phi = 0.45$ and 314–356 K for $\phi = 0.6$ at 60 s.

Fig. 13 shows the spatial distribution of amplitude, power and temperature for beef–oil with SiC–metallic composite support for the three porosities. The sample thicknesses are 0.35, 0.45 and 0.55 cm, respectively. It is interesting to note that, these sample thicknesses are identical to that for alumina–metallic support. Furthermore, as in Fig. 12, stationary electric field has a maxima at the exposed face of the sample and there is a jump in amplitude of the transmitted and reflected waves at the sample–SiC interface. Similarly there is also a jump in the power profile as can be seen from Fig. 13. There is negligible power absorption within the alumina support as seen in Fig. 12 due to the small dielectric response of alumina whereas there is significant power absorption within the SiC support as SiC has a high dielectric loss. Therefore, the power absorption within the sample with SiC–metallic support is smaller than that with alumina–metallic support. The average power absorption for the three cases are 2.13, 1.81 and 1.50 W cm^{-3} respectively. However, the power absorption is still higher than that for some cases with metallic support. In addition, the problem of zero electric field near the metallic support has been eliminated by the presence of composite support and the overall power absorption within the sample has been enhanced compared to metallic support. The temperature within the sample for the three porosities varies within 314–340 K, 312–346 K and 310–348 K at 60 s.

Fig. 14a–e shows the temperature difference (ΔT_b) vs time distribution for beef–oil samples with metallic, ceramic and composite supports for the three porosities 0.3, 0.45 and 0.6. In contrast to beef–air samples, increase in ΔT_b with increase in porosity is quite small for beef–oil samples with various supports. As in beef–air samples, the temperature difference is largest for samples attached with alumina–metallic support. It may be noted that the temperature difference (ΔT_b) for $\phi = 0.6$ at 80 s for beef

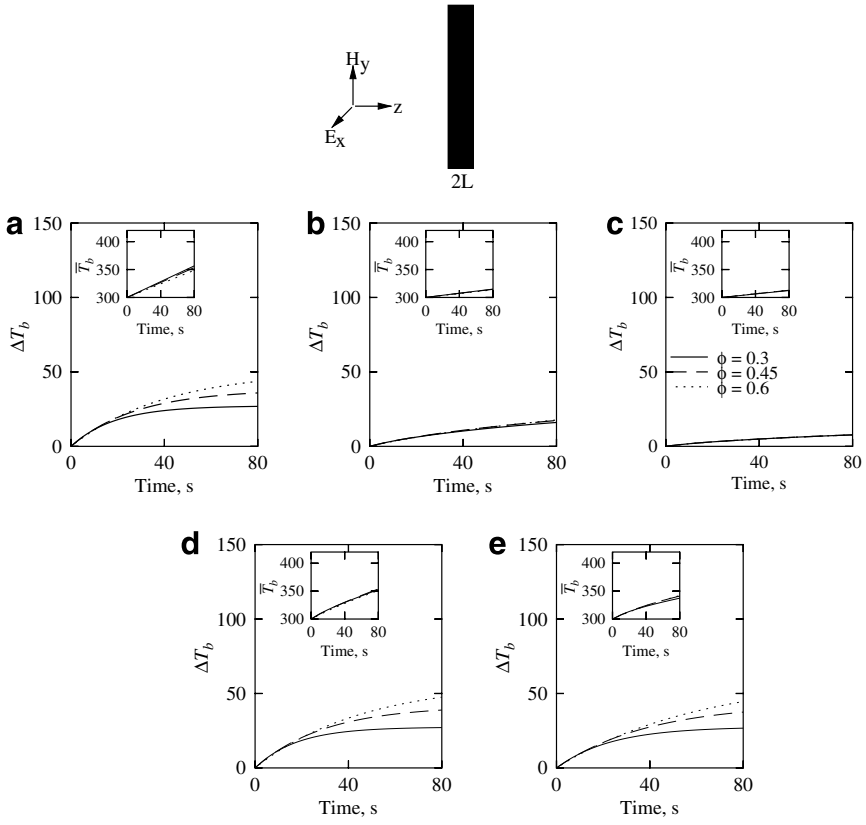

Fig. 14. The temperature difference, ΔT_b (K) vs time (s) for porous beef–air samples ($\phi = 0.3$, 0.45 and 0.6) exposed to microwaves at one face during R_1 mode for (a) metallic support, (b) alumina support, (c) SiC support, (d) alumina–metallic support, (e) SiC–metallic support. The inset shows average temperature, $\overline{T}_b$ (K) vs time (s).

with metallic support, alumina–metallic support, SiC–metallic support, alumina support and SiC support are 43.6 K, 47.5 K and 44.6 K, 17.7 K and 8.9 K, respectively. Thermal runaway may be significant for metallic and composite support cases. However, the higher heating rate would suggest metallic and composite support for an efficient heating policy.

The inset shows the average temperature $\overline{T}_b$ (which indicates the heating rate) vs time. The heating rates are almost the same for samples with metallic and ceramic–metallic composite supports, whereas it is slightly smaller for samples with alumina and SiC supports. The average temperatures at 80 s for beef–oil samples with metallic, alumina–metallic, SiC–metallic, alumina and SiC supports are 348.7 K, 351.1 K, 342 K, 313.4 K and 313.6 K, respectively for porosity $\phi = 0.6$. Therefore, as in beef–air samples metallic and alumina–metallic supports are suitable for efficient thermal processing of beef–oil samples.

4. Conclusions

An extensive analysis of microwave heating of porous beef, beef–air (b/a) and beef–oil (b/o) with metallic, ceramic and composite supports has been carried out with microwave incidence on the left side for three porosities: 0.3, 0.45 and 0.6. A preliminary estimate of the microwave power absorption within the samples, with various support assemblies has been illustrated by plotting the average power against sample thicknesses. The maxima in average power are termed as resonances and the two consecutive resonances are called R_1 and R_2 modes that occur at specific sample thicknesses.

The average power vs sample thickness diagram for b/a samples show that samples with composite supports (alumina–metallic and SiC–metallic) correspond to larger power absorption whereas samples with ceramic supports (alumina and SiC) correspond to smaller power absorption. A mathematical analysis has been carried out to study the role of individual traveling waves on spatial power and temperature distribution for b/a samples attached with metallic, ceramic and composite supports. Unlike ceramic supports, metallic supports do not allow the waves to penetrate through and significant amount of reflection causes stronger stationary waves within the sample. Therefore, the power absorption in samples attached with metallic supports is larger than that with ceramic supports. Although metallic supports enhance the power absorption within the sample, the power absorption is nearly zero at the sample–support interface. This can be obviated by using ceramic–metallic composite supports. An efficient heating strategy has been described based on temperature difference (ΔT_b) and average temperature ($\overline{T}_b$) vs time plot. The heating rate is large for samples with alumina–metallic support with significant thermal runaway especially for higher porosities. Therefore, alumina–metallic support may be recommended as an optimal heating strategy for b/a samples with smaller porosities ($\phi \leqslant 0.45$) and metallic support may be a suitable choice for samples with larger porosities ($\phi \geqslant 0.45$).

Similar to b/a samples, the largest average power absorption is observed for the samples with metallic and alumina–metallic supports. In contrast to b/a samples, less runaway is observed, and temperature difference and heating rate are found to be almost the same for b/o samples with metallic and composite supports. As in to b/a samples, the optimal heating strategy corresponds to metallic or alumina–metallic support for b/o samples.

Overall, the analysis presents an efficient heating strategy for thermal processing of porous substances (b/a or b/o) supported on metallic substrates. Further, the spatial inhomogenity of temperature due to lower power near the metallic support can be enhanced with alumina–metallic composite support.

References

[1] K.G. Ayappa, H.T. Davis, E.A. Davis, J. Gordon, Analysis of microwave heating of materials with temperature-dependent properties, Am. Inst. Chem. Eng. J. 37 (1991) 313–322.
[2] K.G. Ayappa, H.T. Davis, E.A. Davis, J. Gordon, Two-dimensional finite element analysis of microwave heating, Am. Inst. Chem. Eng. J. 38 (1992) 1577–1592.
[3] S.A. Barringer, E.A. Davis, J. Gordon, K.G. Ayappa, H.T. Davis, Effect of sample size on microwave heating rate: oil vs water, Am. Inst. Chem. Eng. J. 40 (1994) 1433–1439.
[4] K.G. Ayappa, H.T. Davis, S.A. Barringer, E.A. Davis, Resonant microwave power absorption in slabs and cylinders, Am. Inst. Chem. Eng. J. 43 (1997) 615–624.
[5] T. Basak, K.G. Ayappa, Influence of internal convection during microwave thawing of cylinders, Am. Inst. Chem. Eng. J. 47 (2001) 835–850.
[6] T. Basak, K.G. Ayappa, Role of length scales on microwave thawing dynamics in 2D cylinders, Int. J. Heat Mass Transfer 45 (2002) 4543–4559.
[7] T. Basak, Analysis of resonances during microwave thawing of slabs, Int. J. Heat Mass Transfer 46 (2003) 4279–4301.
[8] T. Basak, Role of resonances on microwave heating of oil–water emulsions, Am. Inst. Chem. Eng. J. 50 (2004) 2659–2675.
[9] T. Basak, Analysis of microwave propagation for multilayered material processing: Lambert's law versus exact solution, Ind. Eng. Chem. Res. 43 (2004) 7671–7675.
[10] T. Basak, A.S. Priya, Role of ceramic supports on microwave heating of materials, J. Appl. Phys. 97 (2005). Art. No. 083537.
[11] T. Basak, A. Meenakshi, Influence of ceramic supports on microwave heating for composite dielectric food slabs, Am. Inst. Chem. Eng. J. 52 (2006) 1995–2007.
[12] T. Basak, A. Meenakshi, A theoretical analysis on microwave heating of food slabs attached with ceramic plates: role of distributed microwave incidence, Food Res. Int. 39 (2006) 932–944.
[13] T. Basak, K. Aparna, A. Meenakshi, A.R. Balakrishnan, Effect of ceramic supports on microwave processing of porous food samples, Int. J. Heat Mass Transfer 49 (2006) 4325–4339.
[14] S. Oh, K. Tajima, M. Ando, T. Ohji, Fabrication of porous Al_2O_3 by microwave sintering and its properties, Mater. Lett. 48 (2001) 215–218.
[15] X. Wang, H. Fan, Y. Xiao, X. Zhang, Fabrication and characterization of porous hydroxyapatite/β-tricalcium phosphate ceramics by microwave sintering, Mater. Lett. 62 (2006) 4709–4714.
[16] D.W. Lyons, J.D. Hatcher, J.E. Sunderland, Drying of a porous medium with internal heat generation, Int. J. Heat Mass Transfer 15 (1972) 897–905.

[17] P. Glouannec, D. Lecharpentier, H. Noel, Experimental survey on the combination of radiating infrared and microwave sources for the drying of porous material, Appl. Thermal Eng. 22 (2002) 1689–1703.
[18] P. Ratanadecho, K. Aoki, M. Akahori, Influence of irradiation time, particle sizes, and initial moisture content during microwave drying of multi-layered capillary porous materials, J. Heat Transfer-Trans. ASME 124 (2002) 151–161.
[19] P. Salagnac, P. Glouannec, D. Lecharpentier, Numerical modeling of heat and mass transfer in porous medium during combined hot air, infrared and microwaves drying, Int. J. Heat Mass Transfer 47 (2004) 4479–4489.
[20] H. Ni, A.K. Datta, K.E. Torrance, Moisture transport in intensive microwave heating of biomaterials: a multiphase porous media model, Int. J. Heat Mass Transfer 42 (1999) 1501–1512.
[21] G.H. Chen, W. Wang, A.S. Mujumdar, Theoretical study of microwave heating patterns on batch fluidized bed drying of porous material, Chem. Eng. Sci. 56 (2001) 6823–6835.
[22] L. Wang, D. Sun, Recent developments in numerical modeling of heating and cooling processes in the food industry: a review, Trends Food Sci. Technol. 14 (2003) 408–423.
[23] D.D. Dincov, K.A. Parrott, K.A. Pericleous, Heat and mass transfer in two-phase porous materials under intensive microwave heating, J. Food Eng. 65 (2004) 403–412.
[24] A.K. Datta, Porous media approaches to studying simultaneous heat and mass transfer in food processes. II: property data and representative results, J. Food Eng. 80 (2007) 96–110.
[25] H. Fricke, The complex conductivity of a suspension of stratified particles of spherical or cylindrical form, J. Phys. Chem. 59 (1955) 168–174.
[26] A. Chatterjee, T. Basak, K.G. Ayappa, Analysis of microwave sintering of ceramics, Am. Inst. Chem. Eng. J. 44 (1998) 2302–2311.
[27] J.N. Reddy, An Introduction to the Finite Element Method, McGraw-Hill, New York, 1993.